Journal of Alloys and Compounds 600 (2014) 146–150

Contents lists available at ScienceDirect

Journal of Alloys and Compounds

journal homepage: www.elsevier.com/locate/jalcom

Facile one-step synthesis and photoluminescence properties of Ag–ZnO core–shell structure

HongJu Zhai [a,b], LiJing Wang [a], DongLai Han [c,d], Huan Wang [a], Jian Wang [c,d], XiaoYan Liu [b], Xue Lin [a], XiuYan Li [b], Ming Gao [b], JingHai Yang [b,*]

[a] Key Laboratory of Preparation and Applications of Environmental Friendly Materials of the Ministry of Education, Jilin Normal University, Siping 136000, Jilin Province, PR China
[b] Key Laboratory of Functional Materials Physics and Chemistry of the Ministry of Education, Jilin Normal University, Siping 136000, Jilin Province, PR China
[c] Changchun Institute of Optics, Fine Mechanics and Physics, Chinese Academy of Sciences, Changchun 130033, China
[d] University of Chinese Academy of Sciences, Beijing 100049, China

ARTICLE INFO

Article history:
Received 13 December 2013
Received in revised form 16 February 2014
Accepted 17 February 2014
Available online 26 February 2014

Keywords:
Ag–ZnO core-shell structure
Photoluminescence
Solvothermal

ABSTRACT

Ag–ZnO core–shell structures were gained via one-step solvothermal process. The products were characterized by means of X-ray diffraction (XRD), transmission electron microscopy (TEM), Raman spectroscopy, photoluminescence (PL) and UV–vis spectroscopy, respectively. It was shown that the properties were greatly changed compared to pure ZnO from the PL and Raman spectra, which indicated the strong interfacial interaction between ZnO and Ag. The work provides a feasible method to synthesize Ag–ZnO core–shell structure photocatalyst, which is promising in the further practical application of ZnO-based photocatalytic materials.

1. Introduction

In recent years, the engineering of materials in nanometer scale has become an emerging interdisciplinary field, based on physics, chemistry, biology and materials science [1–4]. Meanwhile, owing to the possibility of the combination and integration of material properties, tailored and multifunctional nanostructured materials are at the research forefront of nanomaterials. They have aroused special interests in scientific research, owing to their tailored properties in catalysis, luminescence, magnetics and biology [5–8]. Currently, efforts have been focused on the composite particles with a metallic core–shell structure, especially noble metal core–shell structure, because of their unique optical properties in the visible spectral range [9]. Among the various materials, ZnO is one of the most promising oxide semiconductor materials for applications in the field of optics and optoelectronics [10]. It is a transparent wide bandgap semiconductor compound (Eg = 3.37 eV) with a large exciton binding energy (60 meV), showing high luminescence efficiency, biological imaging, as well as photocatalytic properties [11–14]. Additionally, recent studies have shown that ZnO exhibits many novel nanoscale structures, such as nanorods, nanowires, nanobelts, nanotubes and so forth [15–19], which open up new prospects for applications in nanoscience. However, the recombination of photogenerated charge carriers and low surface area weaken its application in this field. When Ag and ZnO nanoparticles formed core–shell structure, the properties of ZnO nanoparticles would be modified, especially the luminescent properties. It is expected to construct such Ag–ZnO core–shell structures to exert novel optical properties [3]. However, even though some preparation methods of Ag–ZnO heterostructure have been reported, such as deposition–precipitation chemical reduction, photolysis reaction and a facile electrospinning method [20–22], they have not been widely applied in certain fields, because of the strict reaction conditions, lower yields, and it is very difficult to form a tight attachment between the core Ag and the shell of ZnO [20]. In this paper, we propose a one-step, simple method for the synthesis of Ag–ZnO core–shell structure, and its photoluminescent properties will be studied in detail.

2. Experimental

2.1. Materials

All the reagents used in the experiments were in analytical grade (purchased from Shanghai chemical Industrial Company) and used without further purification. Deionized water was made in analytical laboratory.

2.2. Preparation of Ag–ZnO core–shell structure

The Ag–ZnO core–shell structures were fabricated by one-step solvothermal process at relative low temperature. For a typical procedure, firstly, 1.500 g zinc acetate dihydrate and 0.020 g silver nitrate were dispersed into 15 mL ethanol with vigorous stirring for about 60 min at room temperature. Secondly, the mixture

* Corresponding author. Tel./fax: +86 434 3294566.
E-mail address: jhyang1@jlnu.edu.cn (J. Yang).

http://dx.doi.org/10.1016/j.jallcom.2014.02.092
0925-8388/

solution was transferred into a Teflon-lined stainless steel autoclave with a capacity of 18 mL. Then sealed and heated the Teflon-lined stainless steel autoclave at 100 °C for 24 h in an ordinary laboratory oven and cooled the autoclave to room temperature. After being thoroughly washed by deionized water several times and dried at 60 °C under air atmosphere, a white layer of the product was finally deposited, and kept for further characterization. Ag–ZnO-PVP was prepared the same procedure as the above-mentioned except the addition of polyvinylpyrrolidone (PVP, M.w. = 20,000) just after the dissolution of silver nitrate and zinc acetate dihydrate, and pure ZnO was made without the addition of $AgNO_3$.

2.3. Sample characterizations

X-ray diffraction (Hitachi, S-570, Japan Rigaku D/max-ga X-ray diffractometer) analysis was employed to characterize the crystalline properties of the resultant Ag–ZnO core–shell structure, the sample was collected on a MAC Science MXP-18 X-ray diffractometer using Cu Kα radiation ($\lambda = 0.154$ nm), obtained at 40 kV, 100 mA and the scanning speed was 10° min^{-1} at a step of 0.02°. Transmission electron microscopy (JEM-2100F, JEOL Inc., Japan) were used to investigate the morphology and composition of the Ag–ZnO core–shell structure. A standard procedure was followed to prepare the sample for the TEM analysis by dispersing the nanostructures in alcohol solvent, meanwhile, a drop of the solution was put on the carbon coated copper grid. Photoluminescence (PL) spectra were performed at room temperature using 325 nm as the excitation wavelength, He–Cd laser as the source of excitation. Raman spectra of nanotubes were obtained by a microlaser Raman spectrometer made in England (LabRam inva) and excited with the 514 nm line of an Ar^+ laser at an incident power of 20 mW. UV–vis absorption spectra were measured on an UV-3101PC UV spectrometer with ethanol as reference.

3. Results and discussion

3.1. Structure characterization

The TEM images of as-prepared Ag–ZnO core–shell structures are shown in Fig. 1(a) and (b). A low-magnified TEM image of this sample shows a high yield of Ag–ZnO core–shell structures, as presented in Fig. 1(a), ZnO nanocrystals are of a hexagonal structure. All these core–shell structures tightly adhere to each other due to an interdigital connection among these ZnO nanocrystals. It can be seen that almost all of the Ag nanoparticle are coated by ZnO nanocrystals. Moreover, Ag aggregates can be hardly found in the TEM image, indicating that all the Ag nanoparticles are dispersed in ZnO nanocrystals to form core–shell structures. Meanwhile, a high-magnified TEM image of an individual Ag–ZnO core–shell structure is shown in Fig. 1(b), demonstrating the core–shell structure is constructed by a Ag core with a diameter of about 20 nm in the center and ZnO shell with an typical length of 80–120 nm around. It can be observed the lattice fringes with interplanar spacing of 0.288 nm corresponding to the (100) plane of ZnO [20].

The powder X-ray diffraction patterns of as-prepared pure Ag nanoparticles and Ag–ZnO core–shell structures are shown in Fig. 2, from which well Ag–ZnO core–shell structure can be identified. The diffraction peaks can be indexed to hexagonal wurtzite ZnO, and no diffraction peaks from any other impurities have been detected. It indicates that Ag–ZnO core–shell structure shows good crystal quality, which exhibits some typical and sharp peaks of ZnO at 2-theta values of 32.5, 34.8, 36.7, 47.2, 56.8 and 67.7° corresponding to the crystal planes (100), (002), (101), (102), (110), (112) and extremely weak peaks of Ag at 2-theta values of 37.8, 44 and 78° corresponding to the crystal planes (111), (220) and (311) respectively. The peaks of Ag are very weak and show a small left-shift compared to pure Ag nanoparticles, indicating the strong interfacial interaction between ZnO and Ag, which is in accordance with the results of TEM.

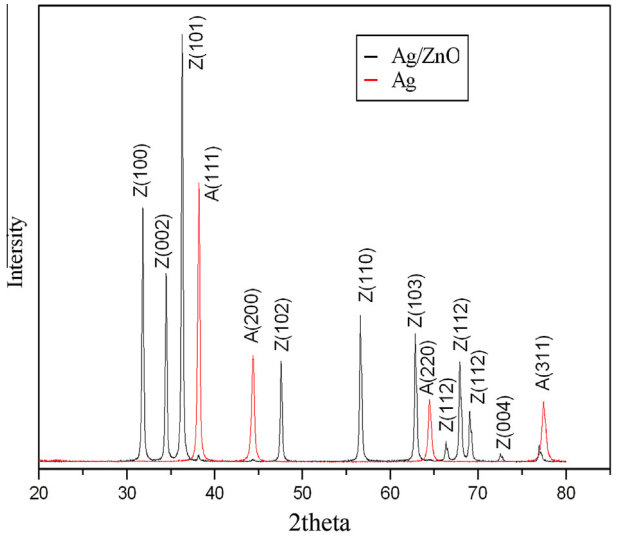

Fig. 2. XRD patterns of as-prepared ZnO and Ag–ZnO (A for Ag and Z for ZnO).

The UV–vis absorption spectra of Ag–ZnO core–shell structure and pure ZnO are shown in Fig. 3, from which two prominent absorption bands are observed in the region 370–500 nm. The former can be assigned to the absorption of the ZnO semiconductor and its corresponding absorption edge is located at around 376 nm [20], while the latter can be attributed to the characteristic absorption of surface plasmon resulting from the metallic Ag. The Ag–ZnO core–shell structure shows a lower absorption compared to pure ZnO, however, its absorption spectrum reveals an expansion from UV to visible area, which indicates potential application of visible light.

The photoluminescent (PL) spectra of the samples have been shown in Fig. 4, which reflects the effect of Ag to ZnO

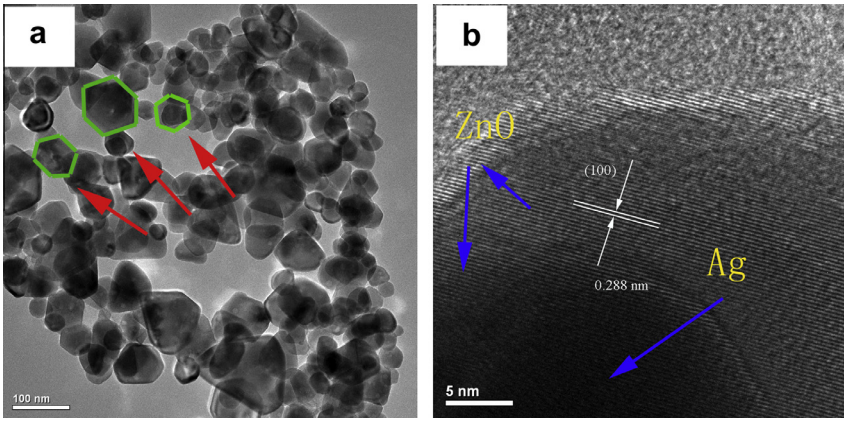

Fig. 1. TEM images of as-prepared Ag–ZnO core–shell structure with low-magnification (a) and high-magnification (b).

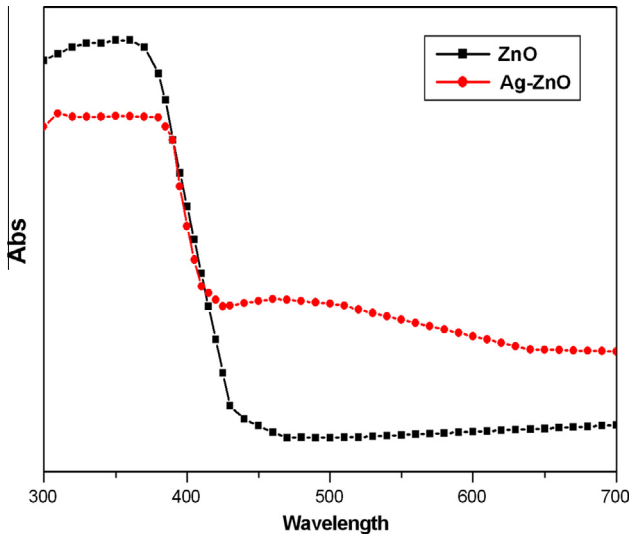

Fig. 3. The UV–vis absorption spectra of Ag–ZnO core–shell structure and pure ZnO.

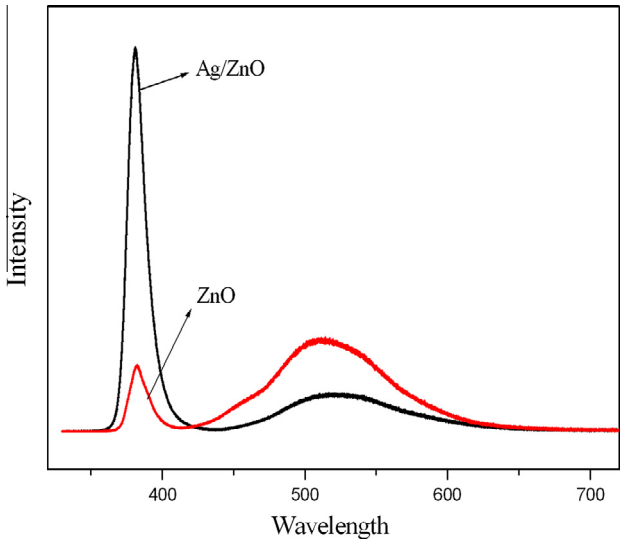

Fig. 4. PL spectra of Ag–ZnO and pure ZnO.

nanoparticles. As can be seen, Ag–ZnO core–shell structure shows obvious increase of UV emission and slight decrease of visible light emission compared to pure ZnO. Generally, the UV emission band is originated from the direct recombination of the free excitons through an exciton–exciton collision process, while the visible emission is due to the zinc or oxygen vacancies and structure defects in ZnO crystals [23–25]. The high intensity ratio of the UV peak to the defect emissions indicates fairly good crystallization of the Ag–ZnO. To account for the increasing intensity of peaks in PL sepctra of Ag–ZnO core–shell structure, the effect of interfacial electron transfer is considered [26]. For Ag–ZnO core–shell structure, O ions saturate the surface states including oxygen vacancies of ZnO, and then, ZnO links on the surface of Ag forming a thin layer as seeds. Furthermore, ZnO nanoparticles are formed at the surface of Ag by crystals growth. When ZnO nanoparticles has connected on Ag nanoparticles under certain percentage, the role of Ag would be larger than that of ZnO, the electron transfer occurs from Ag to ZnO nanoparticles [27]. Therefore, the reduction in combination between electrons and holes for ZnO results in the increase of the PL intensity in Ag–ZnO system [28]. This could be attributed to significant decrease in specific surface areas of Ag–ZnO heterostructures and the surface defect of oxygen vacancies [29], which in turn increases the UV light luminescence.

Two factors are chosen in order to further investigate the effect on the PL spectra of the Ag–ZnO core–shell structure: the calcination temperature and the dispersity. Fig. 5 shows the PL spectra of Ag–ZnO products obtained at various calcination temperatures from 300 to 600 °C calcination and uncalcined samples, which are named S1 to S5 as listed in Table 1 respectively. It can be observed that the PL spectra consists of a sharp and strong UV emission band located at 380 nm together with a weak and suppressed green emission band at 550 nm. Generally, the UV emission band is originated from the direct recombination of the free excitons through an exciton–exciton collision process, while the visible emission is due to the zinc or oxygen vacancies or structure defects in ZnO crystals. The high intensity ratio of the UV peak to the defect emissions indicates fairly good crystallization of the ZnO nanoparticles [30]. It also suggests that the optical properties of ZnO crystals are sensitive to the calcination temperature, when the calcination temperature is low, all peaks are broad and weak, indicating that the particle size of the product is small and its growth is not complete, however, with the calcination temperature increasing from 300 to 600 °C , the primary peak located at 380 nm becomes stronger and sharper, indicating that the increasing calcination temperature leads to a better crystallization and an increase of average particles, suggesting a gradual growth of the nano-particles during the heating process [31–33].

The dispersity of the sample is another factor to the PL spectra of the Ag–ZnO core–shell structure, so PVP was added to explore the mechanism of the overgrowth progress of the Ag–ZnO

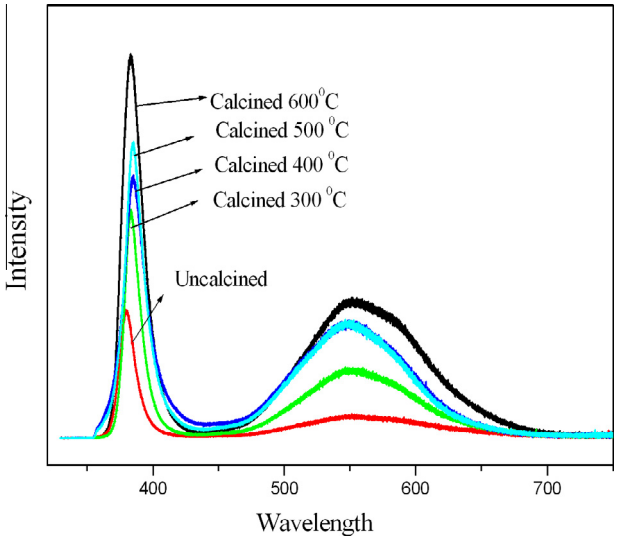

Fig. 5. PL spectra of Ag–ZnO under different calcination temperature.

Table 1
Detail synthesis conditions of the resulted samples at different calcination temperature.

Sample	Calcination temperature	Intrinsic peak intensity and corresponding wavelength (nm)	Defect peak intensity and corresponding wavelength (nm)
S1	Uncalcinated	4500 (380)	200 (550)
S2	300 °C	8200 (380)	2000 (550)
S3	400 °C	9300 (380)	4000 (550)
S4	500 °C	11,000 (380)	4200 (550)
S5	600 °C	14,300 (380)	5000 (550)

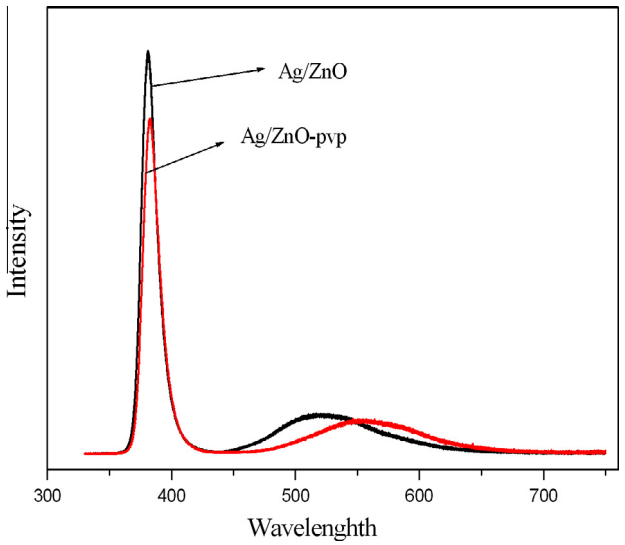

Fig. 6. PL spectra of Ag–ZnO-PVP and pure Ag–ZnO.

core–shell structure. As is shown in Fig. 6, Ag–ZnO core–shell structure with a narrow UV emission band can be assigned to excitonic recombination and the visible emission can be assigned to surface states [34]. Ag–ZnO core–shell structure with PVP absorption reveals red-shift and weak peak. For the broadening and red-shift of surface plasmon absorption, the interfacial coupling between Ag and ZnO nanoparticles may be the reason. It is generally believed that a lower excitonic PL intensity means an enhanced separation and transfer of photoinduced electrons. Once PVP is added to Ag–ZnO core–shell structure, the dispersion of Ag core particle would be enhanced, leading to the separation and transfer of photoinduced electrons [35,36]. Therefore, it is reasonable that the PL intensities of Ag–ZnO core–shell structure with PVP sample is a little lower than that of the sample without PVP.

Fig. 7(a) shows the Raman spectra of pure ZnO nanoparticles, which display three strong and two weak peaks. The peak at 438 cm^{-1} is attributed to optical phonon E_2(high) modes while the peak at 411 cm^{-1} corresponds to the E_1(TO) mode, but it is not obvious. As the characteristic peak of hexagonal wurtzite ZnO, the peak at 438 cm^{-1} is very intensive. The peak at 578 cm^{-1} is attributed to the E_1(LO) mode, which is caused by the defects such as oxygen vacancy, zinc interstitial, or their complexes and free carriers [37]. Meanwhile, the spectrum of the Ag–ZnO core–shell structure is shown in Fig. 7(b), which consists of conventional modes mainly centered at 438, 487, 584, and 663 cm^{-1}. These modes, which mostly reveal the peaks of ZnO, persist in the Ag–ZnO core–shell structure, however, part of their peaks positions are shifted. As can be seen from the spectrum, the presence of the dopants shifts the 438 cm^{-1} and 332 cm^{-1} line towards higher frequencies of 385 cm^{-1} and 487 cm^{-1} respectively, although there are still peaks at 340 $cm^{-1}$and 438 cm^{-1}, they are not obvious, and reveals several additional anomalous modes in the wavenumber range 500–650 cm^{-1}, especially the mode present in the sample at 611 cm^{-1}. We believe that these additional weak modes may be related to the decrease of intrinsic defects created by the modification of Ag to ZnO nanoparticles. Because the Roman spectra are from mostly ZnO nanoparticles but little Ag peaks, perhaps due to the high-density coverage of ZnO on Ag cores. Furthermore, the shifts and additional peaks of Ag–ZnO core–shell structure may also contribute to their structure characteristic [38]. According to the TEM results, the large surface area and high surface roughness imply the pronounced enhancement of surface activity compared with that of bulk crystals, which in turn affects its Raman spectra.

3.2. Mechanism

On the basis of further investigations, a possible formation mechanism is proposed, as is schematically shown in Fig. 8. Ag–ZnO core–shell structure is prepared by a one-step process in which the $Zn(CH_3COO)_2{\cdot}2H_2O$ and $AgNO_3$ are sequentially added into the ethanol and connected through a Zn–O–Ag bond in the precursor. After $Zn(CH_3COO)_2{\cdot}2H_2O$ is dissolved in ethanol solution, the compound breaks down to generate the ZnO nanoparticles under heating conditions. The success of the strategy should be mainly contributed to the two important roles of the ethanol: it could act as a medium for the formation of ZnO nanoparticles, and reduce the Ag ions to form Ag nanoparticles at the same time. In addition, it is well-known that ethanol is a weak reducing agent under high temperature and pressure. When the precursor is treated solvothermally at 100 °C for 24 h, the oxygen vacancy should be generated on the surface of ZnO nanocrystals [39,40]. Also, the reduction of Ag on the surface of ZnO nanocrystals should also occur during the process of solvothermal treatment because pure Ag nanoparticles have been obtained in this synthetic system. The possible reaction formulas for the generation of Ag–ZnO core–shell structure is proposed as the following:

$$Zn(CH_3COO)_2.2H_2O \rightarrow ZnO\downarrow + 2CH_3COOH + H_2O \quad (1)$$

$$2CH_2CH_3OH + O_2 \rightarrow 2CH_3CHO + 2H_2O \quad (2)$$

$$CH_3CHO + 2AgNO_3 + H_2O \rightarrow 2Ag\downarrow + 2HNO_3 + CH_3COOH \quad (3)$$

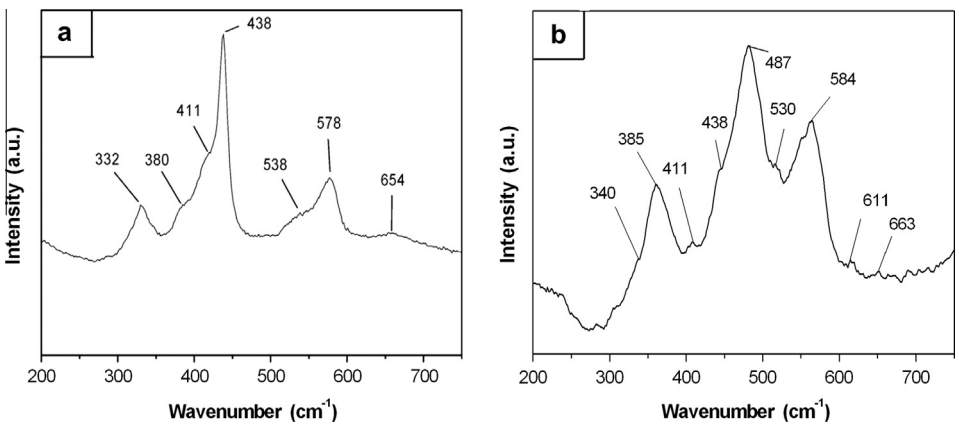

Fig. 7. Raman spectra of pure ZnO (a) and Ag–ZnO core–shell structure (b).

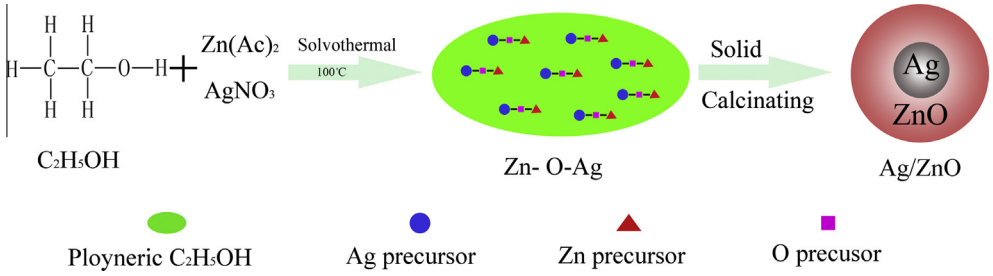

Fig. 8. Schematic diagram for the fabrication of Ag–ZnO core–shell structure.

As it is mentioned above, ZnO is prepared by the decomposition of $Zn(CH_3COO)_2{\cdot}2H_2O$ and the Ag precursor is reduced by ethanol gradually during the solvothermal process, and then a Zn–O–Ag bond should be formed between metallic Ag and ZnO nanocrystals, resulting in the formation of Ag–ZnO core–shell structure with a strong interaction.

4. Conclusions

Ag–ZnO core–shell structure has been successfully prepared by a simple solvothermal process. Its structure and properties were studied and a possible formation mechanism was proposed. Well distributed Ag–ZnO core–shell structure is of a hexagonal crystalline, showing obvious increase of UV emission and decrease of visible light emission compared to that of the pure ZnO. Peaks of PL spectra of the product increased with increasing calcination temperature. The Raman spectrum of Ag–ZnO core–shell structure is similar to that of pure ZnO nanoparticles, but parts of their peaks positions are shifted. All these facts certified that Ag–ZnO core–shell structure is successfully obtained, and has made much difference to the properties of pure ZnO nanoparticles. This method is facile, low-cost and easy for scale production. It provides theoretical basis for the application research of ZnO, and may be the referential experience for synthesis of other semiconductor materials, which have great future prospects in optics, photocatalysis, photovoltaics, and plasmonics.

Acknowledgments

This work is supported by the National Natural Science Foundation of China (Grant Nos. 61308095 and 61378085), National Programs for High Technology Research and Development of China (863) (Item No. 2013AA032202), the Program for the Development of Science and Technology of Jilin Province (Item Nos. 20130102004JC and 20130522071JH), the Program of Siping Technology Bureau (Item No. 2012031), the Program for the Innovation of Youth Talents of Jilin Normal University (Item No. JSDCXRC2011-13), the Program for the masters scientific and innovative research of Jilin Normal University (Item No. 2013027).

References

[1] Q. Zhang, C.G. Tian, A.P. Wu, Y. Hong, M.X. Li, H.G. Fu, J. Alloys Comp. 563 (2013) 269–273.
[2] K.B. Dermenci, B. Genc, B. Ebin, T. Olmez-Hanci, S. Gürmen, J. Alloys Comp. 586 (2014) 267–273.
[3] Y. Caglar, A. Arslan, S. Ilican, E. Hür, S. Aksoy, M. Caglar, J. Alloys Comp. 574 (2013) 104–111.
[4] S. Kaur, B. Singhal, J. Biosci. Bioeng. 113 (2012) 1–4.
[5] A.M.G. Tavares, B.S. Fernandes, S.A. Souza, W.W. Batista, F.G.C. Cunha, R. Landers, M.C.S.S. Macedo, J. Alloys Comp. 591 (2014) 91–99.
[6] J.J. Duan, X.H. Liu, Q.F. Han, X. Wang, J. Alloys Comp. 509 (2011) 9255–9263.
[7] Q.Q. Gao, Q.X. Yu, B. Chen, H. Zhu, J. Alloys Comp. 590 (2014) 446–452.
[8] J.C. Li, Y.F. Li, T. Yang, B. Yao, Z.H. Ding, Y. Xu, Z.Z. Zhang, L.G. Zhang, H.F. Zhao, D.Z. Shen, J. Alloys Comp. 550 (2013) 479–482.
[9] J.H. Yang, J.H. Zheng, H.J. Zhai, X.M. Yang, L.L. Yang, Y. Liu, J.H. Lang, M. Gao, J. Alloys Comp. 489 (2010) 51–55.
[10] H.B. Hu, Z.H. Wang, S.F. Wang, F.W. Zhang, S.P. Zhao, S.Y. Zhu, J. Alloys Comp. 509 (2011) 2016–2020.
[11] L.H. Xu, G. Zheng, M. Lai, S. Pei, J. Alloys Comp. 583 (2014) 560–565.
[12] P. Pawinrata, O. Mekasuwandumrongb, J. Panpranot, Catal. Commun. 10 (2009) 1380–1385.
[13] K.J. Liu, J.Y. Zhang, H. Gao, T.F. Xie, D.J. Wang, J. Alloys Comp. 552 (2013) 299–303.
[14] R.O. Moussodia, L. Balan, C. Merlin, C. Mustin, R. Schneider, J. Mater. Chem. 20 (2010) 1147–1155.
[15] C. Karunakaran, V. Rajeswari, P. Gomathisankar, J. Alloys Comp. 508 (2010) 587–591.
[16] D.Y. Jiang, J.X. Zhao, M. Zhao, Q.C. Liang, S. Gao, J.M. Qin, Y.J. Zhao, A. Li, J. Alloys Comp. 532 (2012) 31–33.
[17] X.T. Yin, W.X. Que, D. Fei, F.Y. Shen, Q.S. Guo, J. Alloys Comp. 524 (2012) 13–21.
[18] D.H. Zhang, X.H. Liu, X. Wang, J. Alloys Comp. 509 (2011) 4972–4977.
[19] H.J. Zhai, J.H. Zheng, J.H. Yang, Y. Liu, M. Gao, Crys. Res. Technol. 45 (2010) 647–650.
[20] Y.H. Zheng, L.R. Zheng, Y.Y. Zhan, X.Y. Lin, Q. Zheng, K.M. Wei, Inorg. Chem. 46 (2007) 6980–6986.
[21] Y.H. Zheng, C.Q. Chen, Y.Y. Zhan, X.Y. Lin, Q. Zheng, K.M. Wei, J.F. Zhu, J. Phys. Chem. C 112 (2008) 10773–10777.
[22] D.D. Lin, H. Wu, R. Zhang, W. Pan, Chem. Mater. 21 (2009) 3479–3484.
[23] J.H. Yang, J. Wang, X.Y. Li, J.H. Lang, F.Z. Liu, L.L. Yang, H.J. Zhai, M. Gao, X.T. Zhao, J. Alloys Comp. 528 (2012) 28–33.
[24] Y. Li, B.P. Zhang, J.X. Zhao, J. Alloys Comp. 586 (2014) 663–668.
[25] Y.R. Guo, F.D. Yu, G.Z. Fang, Q.J. Pan, J. Alloys Comp. 552 (2013) 70–75.
[26] G. Shan, S.J. Zheng, S.P. Chen, Y.W. Chen, Y.C. Liu, Colloid Surf. B 94 (2012) 157–162.
[27] P. Sangpour, F. Hashemi, A.Z. Moshfegh, J. Phys. Chem. 114 (2010) 13955–13961.
[28] M.A. Borysiewicz, M. Wzorek, T. Wojciechowski, T. Wojtowicz, E. Kamińska, A. Piotrowska, J. Lumin. 147 (2014) 367–371.
[29] Y.F. Chen, G.S. Yu, F. Li, J.C. Wei, Appl. Clay Sci. 88 (2014) 163–169.
[30] A. Roguska, M. Pisarek, M. Andrzejczuk, M. Lewandowska, Thin Solid Films 553 (2014) 173–178.
[31] H.X. Chen, J.J. Ding, W.G. Guo, Ceram. Int. 40 (2014) 4847–4851.
[32] C.H. Sui, Z. Lu, T.N. Xu, Opt. Mater. 35 (2013) 2649–2653.
[33] S.A. Ansari, M.M. Khan, M.O. Ansari, J. Lee, M.H. Cho, J. Phys. Chem. C 117 (2013) 27023–27030.
[34] H.R. Liu, G.X. Shao, J.F. Zhao, Z.X. Zhang, Y. Zhang, J. Liang, X.G. Liu, H.S. Jia, B.S. Xu, J. Phys. Chem. C 116 (2012) 16182–16190.
[35] C.L. Ren, B.F. Yang, M. Wu, J. Xu, Z.P. Fu, Y Lv, T. Guo, Y.X. Zhao, C.Q. Zhu, J. Hazard. Mater. 182 (2010) 123–129.
[36] T. Hu, F. Li, K. Yuan, Y.W. Chen, ACS Appl. Mater. Int. 5 (2013) 5763–5770.
[37] Y.C. Liang, X.S. Deng, J. Alloys Comp. 569 (2013) 144–149.
[38] M. Ahmad, E. Ahmed, Z.L. Hong, N.R. Khalid, W. Ahmed, A. Elhissi, J. Alloys Comp. 577 (2013) 717–727.
[39] K.C. Barick, M. Aslam, D. Bahadur, J. Alloys Comp. 587 (2014) 282–286.
[40] S. Guillemin, L. Rapenne, H. Roussel, E. Sarigiannidou, G. Brémond, V. Consonni, J. Phys. Chem. C 117 (2013) 20738–20745.